DIRECTIONAL MULTISCALE MODELING OF IMAGES USING THE CONTOURLET TRANSFORM

Duncan D.-Y. Po and Minh N. Do

Coordinated Science Lab and Beckman Institute
University of Illinois at Urbana-Champaign
Urbana IL 61801
Email: duncanpo@uiuc.edu, minhdo@uiuc.edu

ABSTRACT

The contourlet transform is a new extension to the wavelet transform in two dimensions using nonseparable and directional filter banks. Because of its multiscale and directional properties, it can effectively capture the image edges along one-dimensional contours with few coefficients. This paper investigates image modeling in the contourlet transform domain and its applications. We begin with a detail study of the statistics of the contourlet coefficients, which reveals their non-Gaussian marginal statistics and strong dependencies. Conditioned on neighboring coefficient magnitudes, contourlet coefficients are found to be approximately Gaussian. Based on these statistics, we constructed a contourlet hidden Markov tree (HMT) model that can capture all of contourlets' inter-scale, inter-orientation, and intra-subband dependencies. We experiment this model in image denoising and texture retrieval. In denoising, contourlet HMT outperforms wavelet HMT and other classical methods in terms of both visual quality and peak signal-to-noise ratio (PSNR). In texture retrieval, it shows improvements in performance over wavelet methods for various oriented textures.

1. INTRODUCTION

In image modeling, simple models are constructed to capture the defining characteristics of complex natural images. Accurate models can enhance image processing such as compression, denoising and image retrieval. Because of the inherent difficulty in modeling images directly in space due to their highly complex network of inter-dependencies between image pixels, models are often constructed in certain transform domains such as the Fourier or wavelet domain, where the energy density has a more localized structure.

Recently, various multiscale nonseparable transforms have been researched. These transforms, unlike separable transforms such as wavelets, can efficiently capture the intrinsic geometrical structures in natural images such as smooth contour edges. Candès and Donoho pioneered the *curvelet* representation [1] which is shown to be optimal in a certain sense for functions in the continuous domain with curved singularities. Inspired by curvelets, Do and Vetterli developed the *contourlet* representation [2] based on an efficient two-dimensional nonseparable filter banks that can deal effectively with images having smooth contours. Figure 1 shows the contourlet representation of the "Peppers" image.

Contourlets possess not only the main features of wavelets, namely multiresolution and time-frequency localization, but they also show a high degree of *directionality* and *anisotropy*. Precisely,

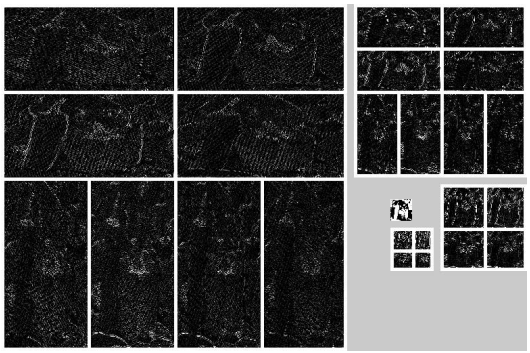

Fig. 1. An example of contourlet transform of the image "Peppers." Small coefficients are colored black while large coefficients are colored white. Larger rectangles correspond to finer subbands.

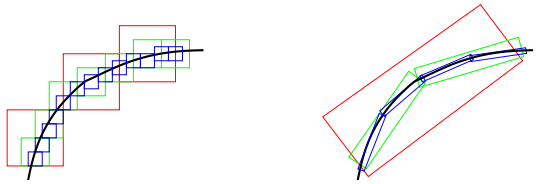

Fig. 2. (a) Wavelet bases have square supports and can only capture points. (b) Contourlet bases have elongated supports and can capture line segments. Contourlets thus can effectively represent a smooth contour with fewer coefficients.

contourlet transform involves basis functions that are oriented at any power of two's number of directions with flexible aspect ratios. With such richness in the choice of bases, contourlets can represent any one-dimensional smooth edges with close to optimal efficiency. For instance, Figure 2 shows that compared with wavelets, contourlets can accurately represent a one-dimensional curve with fewer coefficients.

As a newly developed transform, the characteristics of natural images in the contourlet domain remain largely unknown. More importantly, there has yet to be any attempt to develop models to describe images in contourlet domain. This work takes a first look

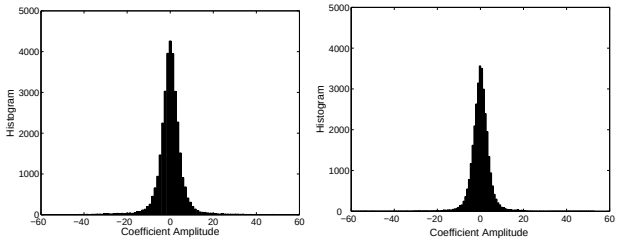

(a) (b)

Fig. 3. Marginal statistics of two finest subbands of the image "Peppers." The kurtoses of the two distributions are measured at (a) 24.50 and (b) 19.40, showing that the coefficients are highly non-Gaussian.

into the subject of contourlet modeling and its applications. Similar to wavelets, contourlet-based models need to take into account the dependencies across scale and space. However, as a "true" two dimensional representation, contourlets allow us to also model the dependencies across directions. In other words, contourlet modeling allows us to jointly model all three fundamental parameters: *scale*, *space* and *direction*, of visual information.

2. STATISTICS

We first study the marginal and joint distributions of the contourlet coefficients of natural images through histogram estimates [3]. Figure 3 shows the marginal distributions of two finest subbands of the contourlet coefficients of the "Peppers" image. The plots show a sharp peak at zero coefficient amplitude and an extended tail to either side of the peak, indicating that the transform is sparse and most coefficients are close to zero. The distributions are highly non-Gaussian, with kurtoses of near 20.

Figure 4 studies the joint statistics by displaying the conditional distributions of finest subbands conditioned on neighboring coefficients across scale $P(X \mid PX)$, space $P(X \mid NX)$ and directions $P(X \mid CX)$, where PX, NX, and CX refer to neighboring coefficients across scale, space and directions respectively. The consistent "bow-tie" shape of all four distributions suggests that contourlet coefficients remain zero-mean regardless of the conditioned magnitude, yet their variance increases as the conditioned magnitude increases. In other words, they are *uncorrelated* yet *dependent*.

We further examine the joint statistics by plotting the conditional distribution $P(X \mid PX = px)$, $P(X \mid NX = nx)$ and $P(X \mid CX = cx)$ where px, nx, and cx are some known values, as shown in Figure 5. The distributions have kurtosis measures close to the Gaussian value of 3, implying contourlets are conditionally Gaussian. This suggests that some form of mixture Gaussian model is appropriate.

3. MUTUAL INFORMATION

To obtain a quantitative characterization of joint statistics, we use *mutual information* as a dependence measure [4, 5]. We estimated the mutual information non-parametrically through histograms. Specifically, we use the estimator

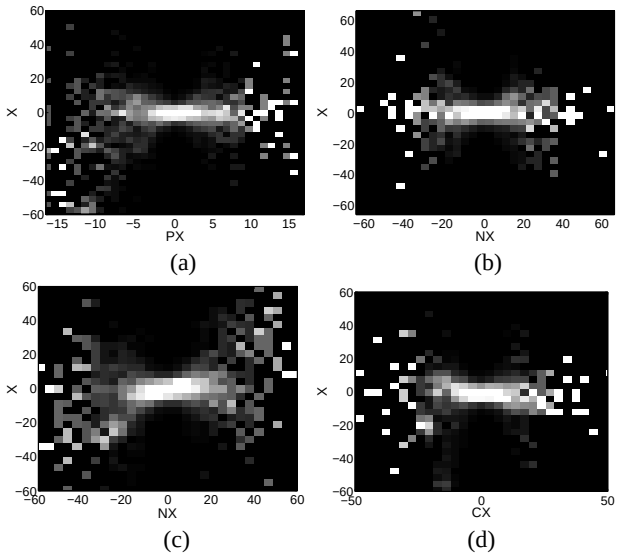

(a) (b) (c) (d)

Fig. 4. Conditional distribution of a finest subband of "Peppers," (a) $P(X \mid PX)$, (b) $P(X \mid NX)$ on the left neighbor, (c) $P(X \mid NX)$ on the up neighbor, (d) $P(x \mid CX)$.

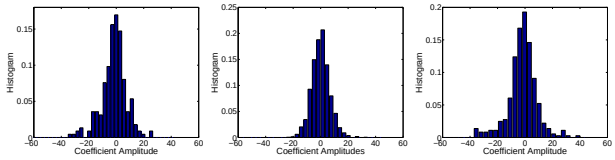

(a) (b) (c)

Fig. 5. Conditional distribution of the coefficients of a finest subband of "Peppers" (a)$P(X \mid PX = px)$, (b)$P(X \mid NX = nx)$, (c)$P(X \mid CX = cx)$. The kurtoses of the distributions are measured at 3.90, 2.90, and 2.99, respectively.

$$\hat{I}(X;Y) = \sum_{i,j} \frac{k_{ij}}{N} \log \frac{k_{ij} N}{k_i k_j} - \frac{(I-1)(J-1)}{2N} \qquad (1)$$

where X and Y are the contourlet coefficients between which we want to estimate the mutual information, k_{ij} is the number of coefficients in a subband observed in cell (i, j), $k_i = \sum_j k_{ij}$ and $k_j = \sum_i k_{ij}$ are the marginal distribution histogram estimates, and N is the total number of coefficients in the subband considered. I and J are the number of histogram cells along the X and Y direction respectively. Note that the first term is the histogram estimate and the second term is a partial bias correction term. Even after the bias is partially removed, the residual bias causes the estimator to underestimate the mutual information and can only serve as its lowerbound.

Table 1 shows the estimate results for various images. We have found that contourlet coefficients of natural images show the highest intrasubband dependencies, followed by rather high inter-orientation dependencies, which is followed by lower inter-scale

Table 1. Mutual information estimate. PX, NX, CX refer to coefficients across scale, space, and directions respectively.

	Lena	Barbara	Peppers
$I(X;PX)$	0.11	0.14	0.10
$I(X;NX)$	0.23	0.58	0.17
$I(X;CX)$	0.19	0.39	0.14
$I(X;PX,NX)$	0.24	0.58	0.17
$I(X;NX,CX)$	0.26	0.59	0.20
$I(X;PX,CX)$	0.21	0.40	0.16
$I(X;PX,NX,CX)$	0.26	0.59	0.20

dependencies. This is especially true for images with higher texture details such as "Barbara." It is also observed that $P(X \mid PX, NX, CX) \approx P(X \mid NX)$, indicating that intra-subband dependency dominates over other dependencies, and conditional on neighboring coefficients, other coefficients do not provide significant additional information about the coefficient. The non-zero mutual information indicates contourlet coefficients show significant inter-scale, intra-subband, and inter-orientation dependencies, with intra-subband dependencies the strongest.

4. HIDDEN MARKOV TREE MODEL

Based on the conditional Gaussian property and the strong dependencies of contourlets, we develop a *contourlet hidden Markov tree (HMT) model* [6]. The software for the implementation of this model can be downloaded from http://www.ifp.uiuc.edu/˜minhdo. Similar to the wavelet HMT model [7], each coefficient is associated with a hidden state variable and conditioned on its state, it is normally distributed with the corresponding variance specified by the state. We define coefficients at the same spatial location in two adjacent scales as parents (in coarser scale) and children (in finer scale). The model accounts for dependencies by establishing links between the *hidden state variables* of parent and child coefficients across scales and imposing a state transition probability matrix on each link. As each parent coefficient has four children, the model has a quad-tree dependence structure. The quad-tree structure allows for direct modeling of inter-scale dependencies and indirect modeling of the dependencies between neighboring coefficients within the same subband, via their links to their common ancestors higher up in scale. As in wavelet HMT, the model parameters can be trained using a fast expectation maximization (EM) algorithm.

While wavelet HMT *only* models inter-scale and intrasubband dependencies, contourlet HMT can also capture dependencies *between adjacent orientations*. Figure 6 illustrates this difference. For wavelets, all children of the same parent are always in the same subband, while for contourlets, children of the same parent can be in adjacent directions. Thus, for contourlets, coefficients in adjacent directions can fall within the same tree and their dependencies will then be captured.

5. DENOISING

We apply the contourlet HMT model in denoising zero-mean additive white Gaussian noise. Given a noisy image, we first obtain the model of the corresponding clean image θ_u by subtracting the noise power from the model variances in the noisy image model

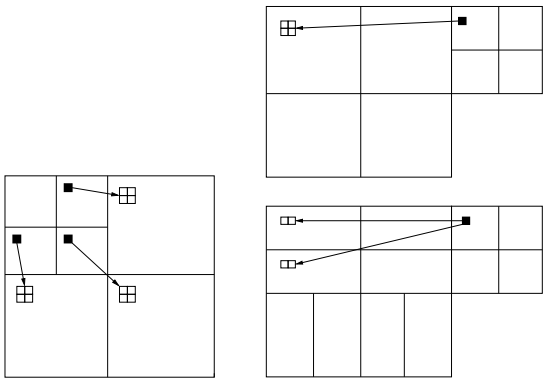

Fig. 6. Parent-children relationship for (a) wavelets and (b) two possible contourlets structures. Black squares represent parent coefficients with white squares as their children. Notice for the bottom contourlet structure, a parent coefficient can have its children spread over two subbands.

θ_v. Noting that white noise in the contourlet domain is correlated due to overcompleteness, we proceed to estimate the j^{th} coefficient in the i^{th} subband

$$E[\vec{u}_{ij} \mid \vec{v}_{ij}, \boldsymbol{\theta_u}] = \sum_m p(S_{ij} = m \mid \vec{v}_{ij}, \boldsymbol{\theta_u}) \times (\sigma^2_{i,m} I) \times (\sigma^2_{i,m} I + \Sigma_n)^{-1} \times \vec{v}_{ij} \quad (2)$$

where $\vec{u}_{i,j,k}$ and $\vec{v}_{i,j,k}$ are respectively the set of clean and noisy coefficients that fall within an arbitrarily-sized local neighborhood window centered at the k^{th} coefficient in the j^{th} subband in the i^{th} scale, $p(S_{ij} = m \mid \vec{v}_{ij}, \boldsymbol{\theta_u})$ is the state likelihood of state m, $\sigma^2_{i,m}$ is the model variance, and Σ_n is the noise covariance matrix. I denotes the identity matrix. Note that a local window of coefficients, rather than a single coefficient, is used in the equation because noise is correlated in the contourlet domain.

The results are highly promising. Contourlets can preserve edges and lines better than wavelets and also produces superior peak signal-to-noise ratio (PSNR) and visual quality in the denoised images. Figure 7 shows an example in the "Zelda" image. This result shows that contourlet HMT gives the best visual quality and PSNR among various classical and wavelet denoising schemes. It successfully removes much noise while also retains the sharp features of the original image.

6. TEXTURE RETRIEVAL

The contourlet HMT model is also applied to content-based texture retrieval. In contourlet texture retrieval, we extract from each texture image in the database and the query image its contourlet HMT model parameters. The Kullback-Liebler distance (KLD) between the query image model and each database image model is then measured and the database images that give the smallest KLD are retrieved.

We experiment on the Brodatz texture database. Comparing the wavelet and contourlet HMT schemes, the average retrieval rate of the contourlet HMT method is 93.27%, higher than the 90.87% of the wavelet HMT method. The top row of Figure 8

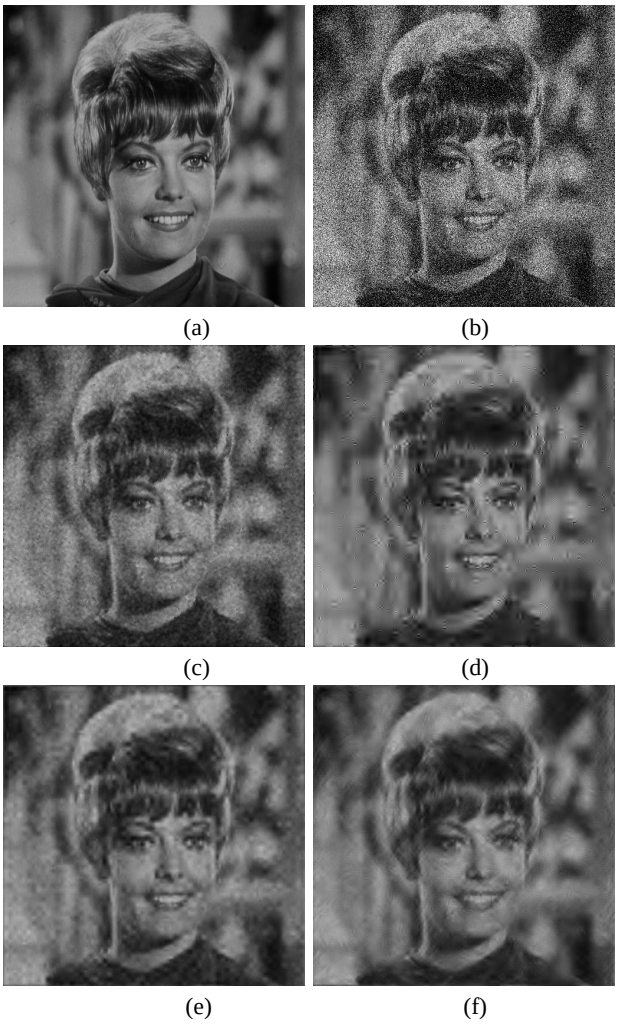

Fig. 7. Denoising results of "Zelda"image: (a) "Zelda" image, (b) noisy image ($\sigma_n = 51$, PSNR = 14.607), (c) wiener2 (PSNR = 25.780), (d) wavelet thresholding (PSNR = 26.046), (e) wavelet HMT (PSNR = 27.631), and (f) contourlet HMT (PSNR = 27.707).

shows the texture images that are better retrieved by wavelets than contourlets by at least 5%, and the bottom part displays the images better retrieved by contourlets by at least 5%. Observe that the top-row images all have dominant vertical or horizontal image components, while the bottom images show more diverse directional components (such as circular or irregular shapes). This shows the superior quality of contourlets in capturing directional information. The difference in retrieval rates between contourlet and wavelet HMT can vary from fractions of a percent up to near 20%. In general, the contourlet HMT retrieval system gives satisfactory texture retrieval performance with retrieval rates typically above 80% for most textures.

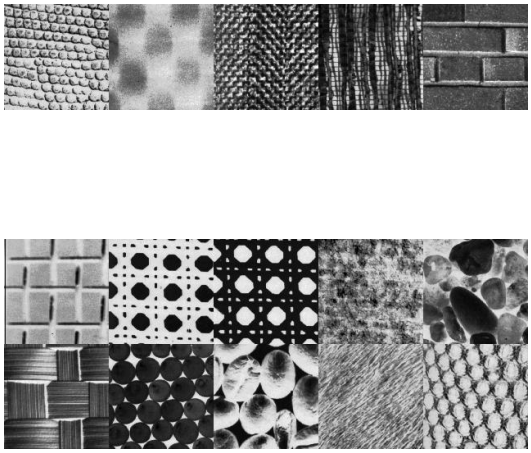

Fig. 8. Texture retrieval results. The top row shows the textures that are better retrieved by wavelets than by contourlets by at least 5%. The bottom two rows show the textures that are better retrieved by contourlets than by wavelets by at least 5%.

7. CONCLUSION

We have developed a new image model defined in the contourlet transform domain. The contourlet HMT model enables us to capture contourlets' conditionally Gaussian and dependence properties across all of image scale, space and directions. We have shown the model's usefulness in denoising and texture retrieval where it gives improved performance over classical methods including wavelet HMT.

8. REFERENCES

[1] E. J. Candés and D. L. Donoho, "Curvelets - a surprisingly effective non-adaptive representation for objects with edges," in *Curve and Surface Fitting*, C. Rabut A. Cohen and L. L. Schumaker, Eds. Vanderbilt University Press, 1999.

[2] M. N. Do and M. Vetterli, "The contourlet transform: an efficient directional multiresolution image representation," submitted to *IEEE Trans. on Image Processing*, 2003.

[3] E. P. Simoncelli, "Modeling the joint statistics of images in the wavelet domain," in *Proc. SPIE* 44^{th} *Annual Meeting (Denver, CO)*, July 1999.

[4] J. Liu and P. Moulin, "Information-theoretic analysis of interscale and intrascale dependencies between image wavelet coefficients," *IEEE Trans. on Image Processing*, vol. 10, no. 10, pp. 1647–1658, November 2001.

[5] T. M. Cover and J. A. Thomas, *Elements of Information Theory*. New York, NY: John Wiley and Sons, Inc., 1991.

[6] D. D.-Y. Po and M. N. Do, "Directional Multiscale Modeling of Images using the Contourlet Transform," submitted to *IEEE Trans. on Image Processing*, 2003.

[7] M. S. Crouse, R. D. Nowak, and R. G. Baraniuk, "Wavelet-based statistical signal processing using hidden markov models," *IEEE Trans. on Info. Theory*, vol. 46, pp. 886–902, April 1998.